Cracking Problems in Wind Turbines

Javier Rodríguez[1], Francisco Riera[1], Joaquín Martí[1],
Pablo Carretero[2], and Alicia Álvarez[2]

[1]Principia, Madrid, Spain
[2]Argos, Madrid, Spain

***Abstract**: By their very nature, wind turbines are subjected to many variable and cyclic loads and, consequently, they are prone to experiencing fatigue cracking problems in various parts of the turbine. Examples include the aluminium rings (alurings) of the blades of several commercial wind turbines, the gears of the yaw control mechanism and even the main rack supporting all the equipment.*

Principia has used numerical simulation with Abaqus and fe-safe to study the origin of many of those cracks, determine their ability to propagate, and analyse the merits of various strategies proposed to solve existing problems or prevent their future occurrence. Among the technologies involved, besides local stress and strain fatigue initiation criteria, are critical distance methods and crack representations based on the extended finite element method (XFEM) to assess the growth behaviour.

The paper concentrates on two of the cases studied, that of the alurings and that of the yaw drive gears. It describes the methodology used for analysing the problem, the results obtained from the simulations and the conclusions reached.

***Keywords**: Wind Turbines, Crack Initiation, Crack Propagation, Fatigue, Alurings, Gears.*

1. Introduction

Two different problems are discussed in the present paper, both of which involve fatigue cracks developed in wind turbines. The first problem has been noted to arise in the aluminium rings (alurings) of the blades of several commercial wind turbines; the alurings connect the blades to their pitch control mechanism. The second problem concerns the gear rim of the yaw control system; its case-hardened teeth are subjected to large variable loads and may undergo damage as a consequence.

In the case of the alurings, a tentative solution had already been proposed. In that situation, once the available information about the problem had been carefully studied, the procedure followed consisted in, first, constructing and analysing models with Abaqus (SIMULIA, 2016a), for both the original and the modified configurations, taking into account the bolt pre-stressing and the fatigue loads. This was then followed by analyses with fe-safe (SIMULIA, 2016b) to determine the fatigue life using the Brown-Miller algorithm. In this communication, only the analysis of the original design is reported.

In the case of the gear rim of the yaw-control mechanism, the teeth are case hardened. The strategy followed consisted in using Abaqus to study the stresses and plastic deformations in the gear teeth. Following that, fracture mechanics analyses were carried out to determine the ability of representative cracks to propagate; this was done by comparing their stress intensity factors with the lower limit provided by Paris law.

2. Cracks in the alurings

2.1 Description of the problem

The aluring connects the root of the blade to the pitch control system, as schematically shown in Figure 1. It is made of aluminium 5083 and connected through 60 M20 bolts class 10.9. Figure 2 presents two views of the aluring, which has an inner radius of 440 mm and a thickness of 40 mm. At the other end it is linked to the blade with epoxy reinforced with unidirectional glass fibres (Figure 3). No structural credit is given to the fill or the outer skin, nor to the silicone used in the retrofit that will be described later.

Figure 4 shows the countersunk end of a bolt hole. Fatigue cracks were detected around the countersinking, propagating outwards and perpendicularly to the hole axis. As they lengthen, cracks may affect more than one hole, eventually leading to the failure of the connection and the release of the blade.

The design preload of the bolts is 162 kN. The extreme load (associated with the maximum load during the design life) over a sector spanning two bolts, is 49 kN. As there are 60 bolts at a radius of 460 mm, this corresponds to a bending moment of 338 kNm, compressing one half of the section and stretching the other. It has been conservatively assumed that the fatigue loads are equal to the maximum loads, thus leading to an amplitude range of 676 kNm.

2.2 Analysis of current design

To analyse the design, a model of the sector spanned by a single bolt was constructed with Abaqus (SIMULIA, 2016a). The model includes the aluring, the fibre reinforced plastic of the inner and outer faces, the bolt, and a ring representing the bearing that provides the reaction to the nut. The compressive or tensile radial force applied to the bearing ring is balanced by a distribution of forces at the end, such that the resultant is aligned with the outer face; this assumption has only a minor influence in the analyses, but helps to explain why the cracks tend to appear in the outer region of the countersinking and not in other locations of its perimeter.

The reconstructed geometry appears in Figure 5. The following interactions were considered:

- Contact between the bolt and the hole. The thread was not explicitly modelled, but was defined as a contact taking into account the helical threading with a half-angle of 30º and a 2 mm pitch for the M20 bolt. This leads to a more realistic stress distribution than a rigid connection, but the effect in the present analyses is only minor.

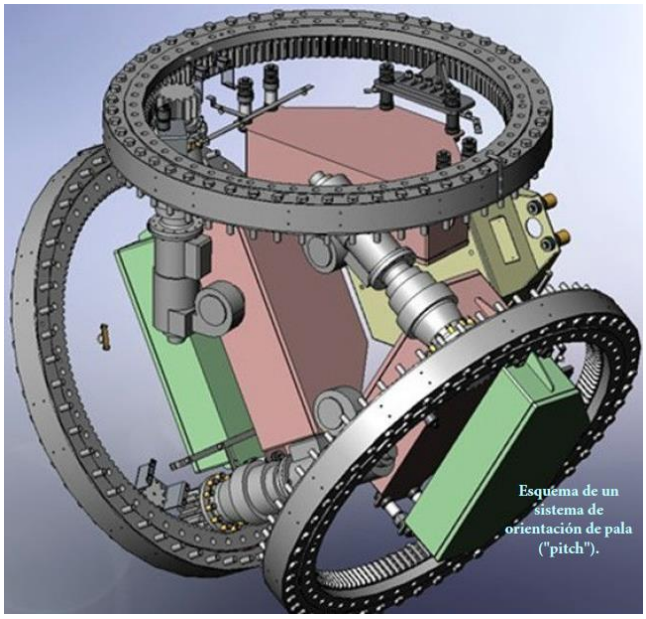

Figure 1. Pitch control system.

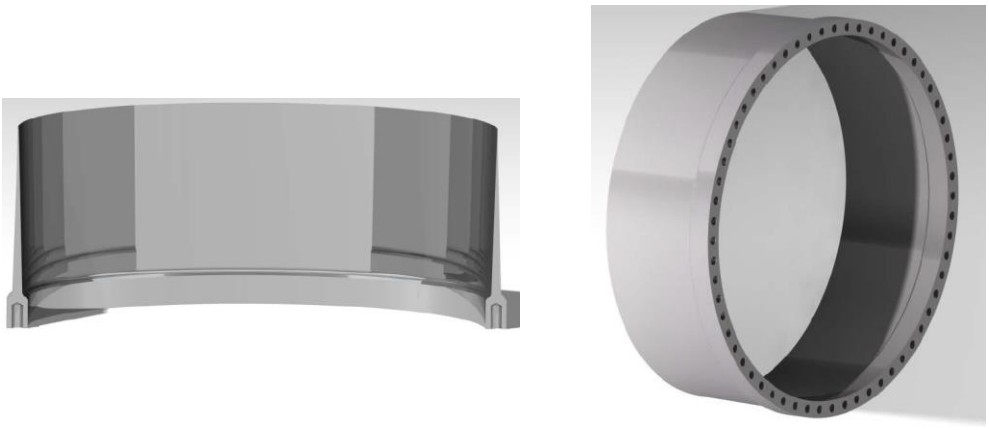

Figure 2. Views of the alluring.

- Contact between the inner surface of the aluring and the outer one of the bearing ring. A friction coefficient of 0.5 was used for the aluminium-steel contact, though again its influence on the results is very limited.
- Rigid connection of the bolt nut to the bearing ring.

– Distributed coupling between the inner extreme face of the bearing and a radially fixed reference node aligned with the outer face to represent the load transfer to the bearing ring.

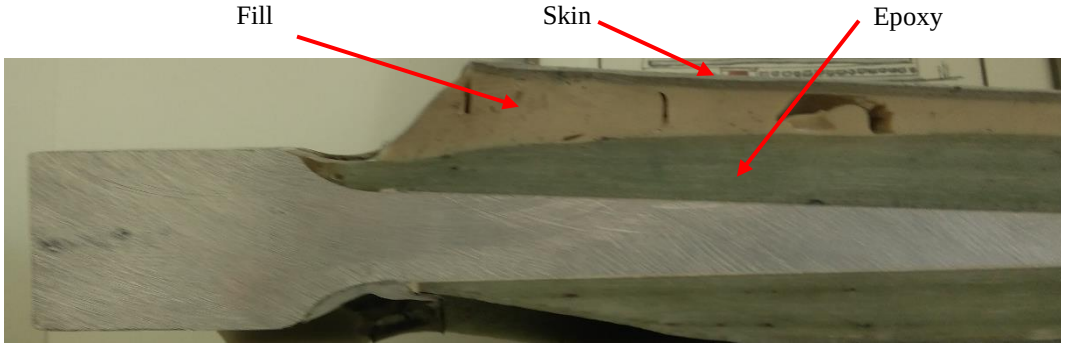

Figure 3. Connection of the aluring to the blade.

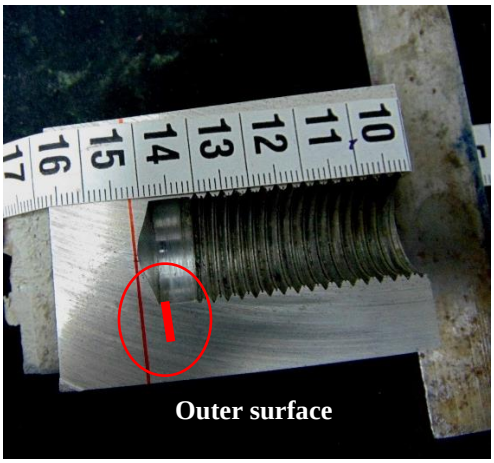

Figure 4. A bolt hole and typical location of cracks.

The model constructed has 114,543 elements, mostly second-order tetrahedra, and 167,112 nodes. The number of degrees of freedom, including those internally added because of contacts, is 529,015. All meridian faces have symmetry conditions applied.

The loads are sequentially imposed in three phases:

a) Preloading of the bolts to 162 kN, followed by fixing the effective bolt length.

b) Tension at the PRFV end with a pressure of 15.2 MPa, corresponding to a radial tension in the model of 24.5 kN.

c) Compression to the same load level.

The countersinking of the bolt hole presents a sharp corner, which implies infinite elastic stresses; this entails damage, even if the cracks were unable to propagate. In such cases, the classical procedures for estimating the fatigue life, such as that described later in section 3, are inadequate and other methods must be used. One of the more efficient ones is that proposed by Taylor (2005), based on stress verifications conducted at certain distance $L/2$ from the surface, as indicated in Figure 6. The critical distance L is a material parameter, which for fatigue verifications is related to the lower limit for propagation ΔK_0 (range of the stress intensity factor for $R \geq 0$ cycling modes) and the lower fatigue limit $\Delta\sigma_0$ (range) corresponding to the same cycling: (3-1)

$$L = \frac{1}{\pi}\left(\frac{\Delta K_0}{\Delta \sigma_0}\right)^2$$

A representative value of ΔK_0 for aluminium 5083 for cycling tension and unloading (R is approximately zero) is 2,9 MPa$\sqrt{\text{m}}$ (Ship Structure Committee, 2007). Goodman's method can be used to correct the stress corresponding to a number of cycles taking into account the mean stress. For the number of cycles of interest this leads to a failure stress of 73.3 MPa and Taylor's critical depth is 0.12 mm.

To evaluate the potential propagation of damage around the countersinking, the mesh was refined in that region to tetrahedra with dimensions on the order of the critical length. Figure 7 shows a detail of the mesh. The critical distance point method states that a fatigue crack will propagate if the stress at a distance $L/2$ below the surface reaches the critical stress, which for alternating stresses is practically 100 MPa (a range of 200 MPa).

Figure 8 does not present stresses extrapolated to the surface, but centroid stresses; the Tresca stresses shown represent differences between the maximum and minimum principal stresses. The jumps across elements do not reflect so much stress discontinuities, but differences in centroid locations between differently oriented contiguous elements. As mentioned, the mesh was generated so that the centroids in the countersinking region are $L/2$ distant from the surface.

The maximum range observed is 486 MPa, considerably larger than the admissible 200 MPa, following the criterion of maximum shear stress (half of Tresca's value); it is therefore expected that the structure will fail before the end of its design life. This corresponds to the reference fatigue scenario, which is fairly conservative, but failure would still be expected if the stress oscillations were reduced by a factor of 2. This result is consistent with the physical observations, as is the critical location for propagation, which is the outer region of the countersinking. If the transition from the cylindrical hole to the countersinking had been smoother, probably it would have been possible to avoid such problems during the design life.

Figure 5. Reconstructed geometry.

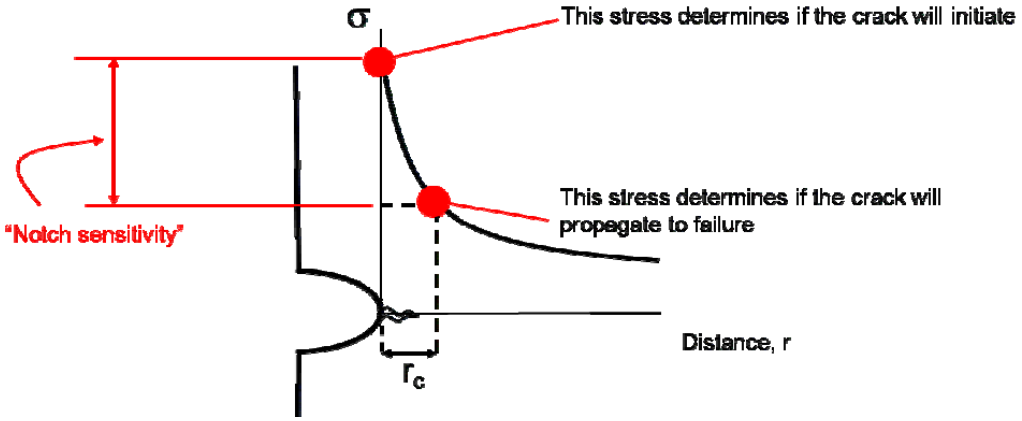

Figure 6. Method of critical distance.

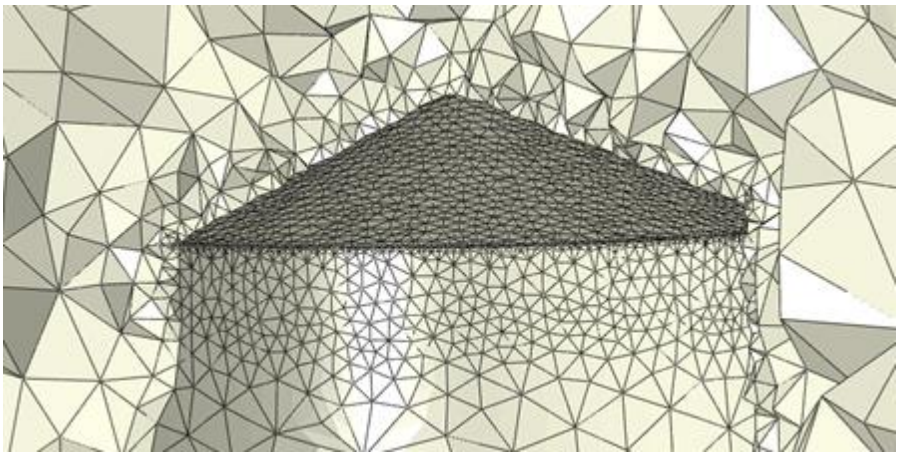

Figure 7. Mesh detail for the critical distance method.

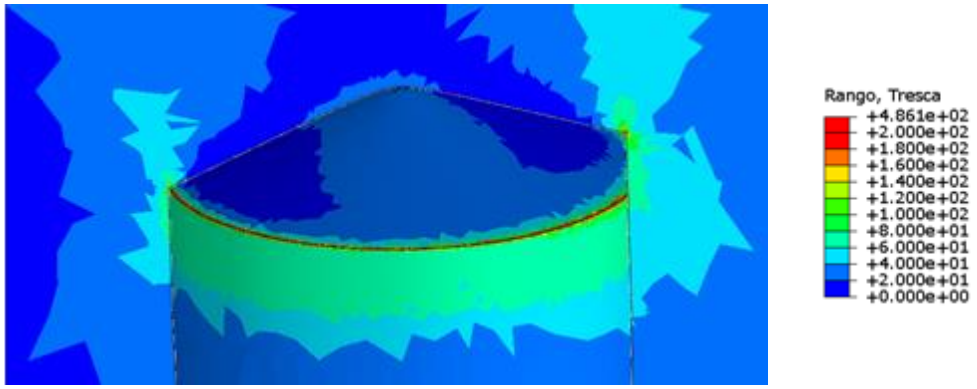

Figure 8. Range of Tresca stresses (MPa).

3. Cracks in the yaw-control gears

3.1 Description of the problem

The torques required to orient the turbine are applied to the yaw-control gear through four pinions, which are not equally spaced along the gear rim. Tables 1 and 2 show the dimensions of the teeth in the yaw-control gear and pinions, respectively.

Table 1. Geometrical parameters of the gear rim.

Module (mm)	14
Number of teeth (-)	174
Pressure angle (º)	20
Modification factor of addendum (-)	+0.5
Reference diameter (mm)	2436
Diameter of the top land (mm)	2475
Height of teeth (mm)	30
Width (mm)	120

The teeth have a hardened surficial layer, about 4 mm thick, and the base material. The Rockwell C hardness values are 53 for the hardened layer and 21 for the base material. This corresponds to an ultimate strength of 1770 MPa (Carbide Depot, 2017) and, assuming the relation with the elastic limit is similar to that in the base material, the elastic limit is 1536 MPa. The elongation can be conservatively estimated as 8.4%, which corresponds to the same energy per unit volume as the non-hardened material.

Table 2. Geometrical parameters of the pinions.

Module (mm)	14
Number of teeth (-)	15
Pressure angle (º)	20
Modification factor of addendum (-)	+0.5
Reference diameter (mm)	210
Diameter of the top land (mm)	249.2
Diameter of the bottom land (mm)	188.088
Initial diameter of the involute (mm)	198.2
Width (mm)	130
Crowning radius (mm)	25,594

The critical stress intensity factor (at fracture) in the base material can be estimated from the Charpy test energy (British Steel, 1998) and the reference value for the brittle or transition behaviour is:

$$K_{25} = 12\sqrt{C_V},$$

where C_V is the Charpy impact energy in J (62.9 in this case) and K_{25} is the fracture toughness in MPa$\sqrt{\text{m}}$ for 25 mm thickness, which is 95.2 MPa$\sqrt{\text{m}}$. The characteristic thickness of the teeth is 44 mm; taking this into account, the critical stress intensity factor is 85.3 MPa$\sqrt{\text{m}}$, or 2697 MPa$\sqrt{\text{mm}}$.

Crack growth is characterised via Göncz *et al* (2010), who give the parameters for Paris law:

$$\frac{da}{dN} = C(\Delta K)^m, \tag{2-2}$$

where a is the crack depth, N is the number of cycles, ΔK is the oscillatory range of the stress intensity factor, and C and m are the growth parameters. The parameters are given in Table 3 for 42CrMo4 steel in units are consistent with MPa and mm.

Table 3. Growth parameters for 42CrMo4 steel.

Material	Hardness	*C*	*m*
Hardened layer	54	$3{,}398 \cdot 10^{-14}$	3,406
Transition	45	$3{,}589 \cdot 10^{-12}$	2,587
Base material	28	$5{,}135 \cdot 10^{-13}$	2,824

For example, for a stress intensity factor of 500 MPa$\sqrt{\text{mm}}$, the growth rate in the hardened material is $5.3 \cdot 10^{-5}$ mm/cycle, while it is only $2.1 \cdot 10^{-5}$ mm/cycle in the base material; thus, for the same stress intensity factor, the growth rate decreases with hardness and in the base material is less than half that in the hardened layer. The values in the table are considered representative, perhaps slightly conservative when the Rockwell C hardness decreases from 28 to 21.

Various types of cracks were detected (Figure 9). It was noticed that those starting in the face of the tooth have difficulty to propagate, but those starting in the flank may do so and eventually go fully across the tooth (Figure 10).

Load information was available from the monitoring system, which allowed characterising the fatigue and extreme loads.

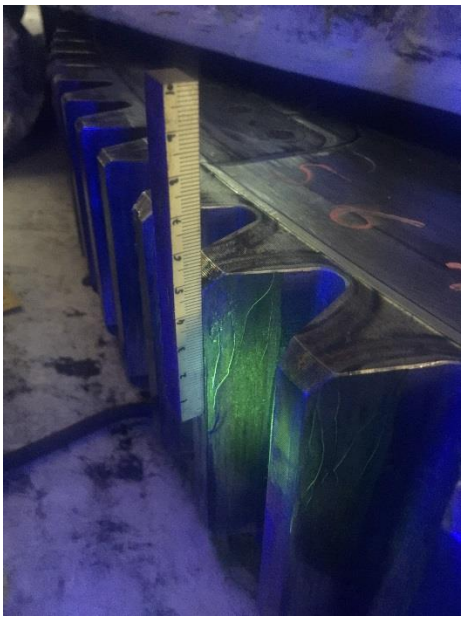

Figure 9. View of representative cracks.

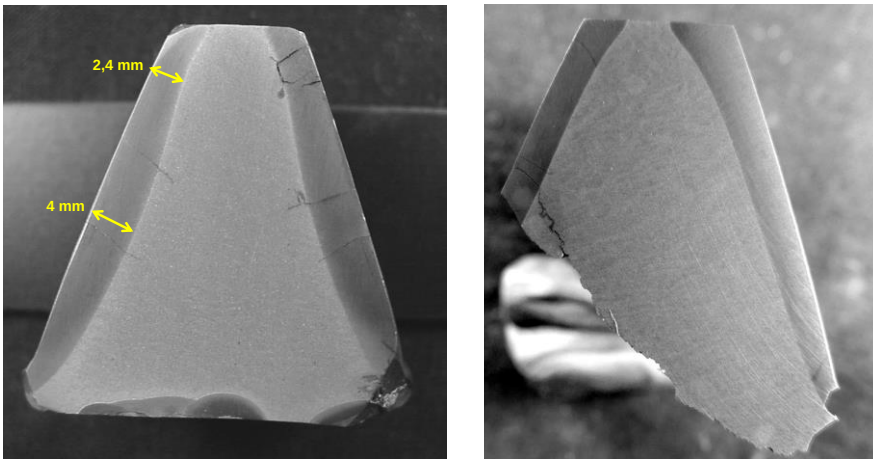

Figure 10. Sections of rim teeth.

3.2 Crack propagation

The geometry shown in Figure 11 was reconstructed with Abaqus/CAE (SIMULIA, 2016c). The teeth evolute was generated with a 10-point spline. Based on the reconstructed geometry, Figure 12 presents views of the meshes used to model the gear rim and pinion teeth. The global mesh, including both gear and pinion, has 289,102 elements, 326,746 nodes, and 940,788 degrees of freedom. It is formed by hexahedral elements with reduced integration. The element size near the surface is 1 mm along the profile, 2 mm in the longitudinal direction, and 0.7 mm in the thickness.

The distance between the centres of the gear and the pinion is 1337 mm and, taking into account that the sum of the addendum correction factors is unity, it corresponds to the sum of the radii of the primitive circumferences plus one module. This distance is very approximately that producing a single contact point during movement.

Two load phases are applied in the analysis. Firstly, a torque is applied at the reference node of the pinion, with the rest of its degrees of freedom restrained and restraining also all degrees of freedom of the reference node of the gear rim. In a second phase the gear is rotated while maintaining the pinion torque.

Figure 13 shows the stresses at various instants. Plastic strains are localized near the top land, suggesting that the cracking experienced is a consequence of the high level of contact stresses.

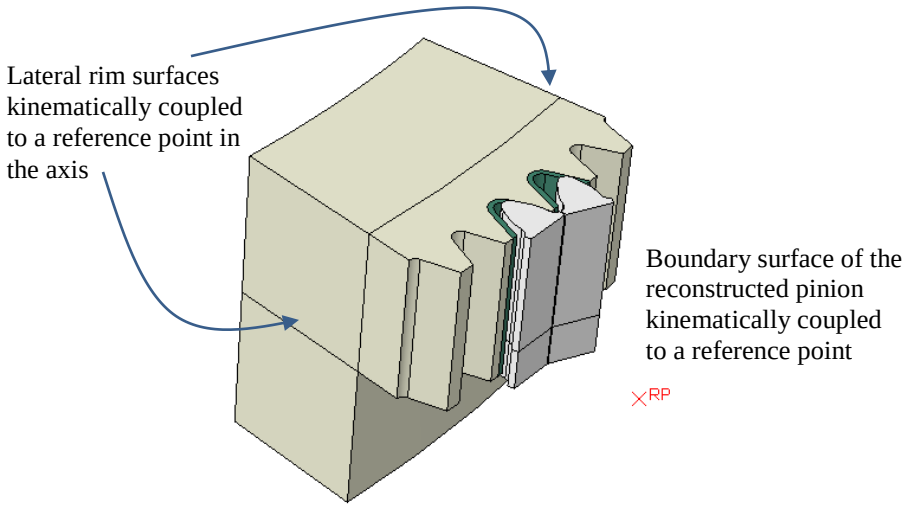

Figure 11. Geometry of the assembly.

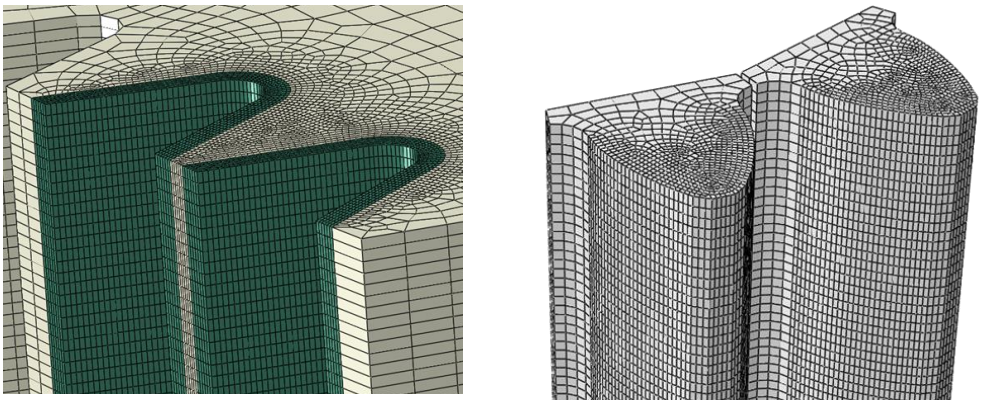

Figure 12. Finite element meshes.

The fe-safe fatigue analyses were based on the Brown-Miller criterion, using Morrow's correction on the basis of parameters estimated by Seeger's method. As can be seen in Figure 14, only small cracks are expected after 10,000 load cycles near the top land.

It is of interest to determine the response when the postulated crack is located 13 mm from the top land (corresponding to the lower point of contact during motion) and the extreme torque is applied. The crack shown in Figure 15 is defined using the XFEM capabilities in Abaqus. The distribution of the stress intensity factor along the crack front is presented in Figure 16 for two crack depths penetrating the core material.

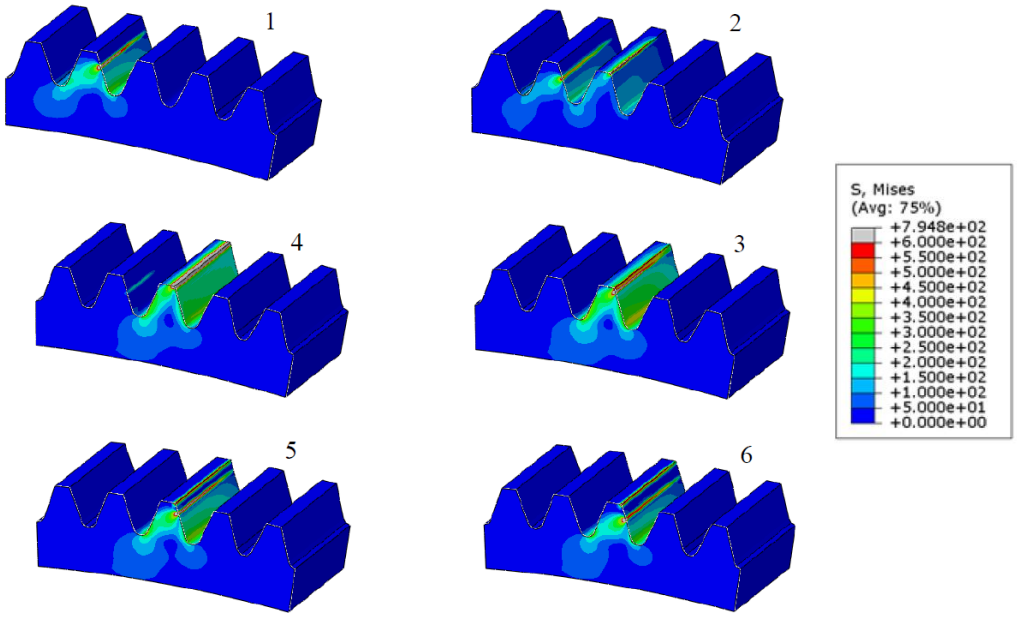

Figure 13. Stresses (MPa) at different instants for 26,1 kNm (cut at max. crowning).

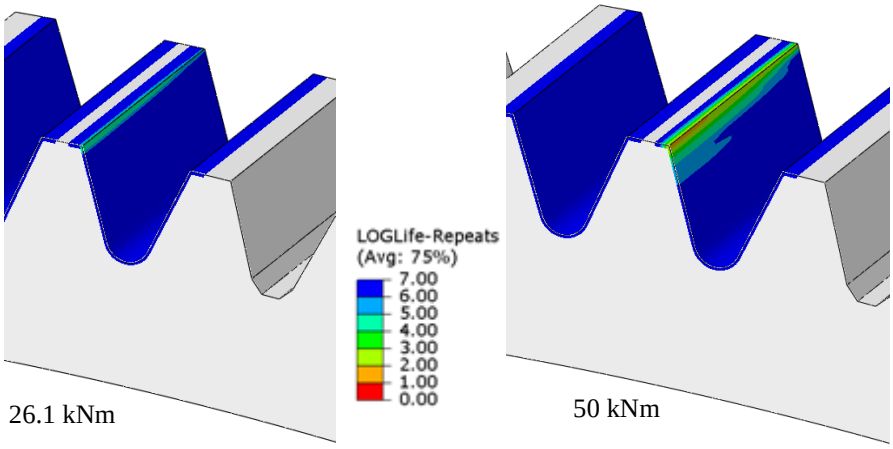

Figure 14. Fatigue life (number of cycles).

Maintaining the assumption of a linear relation in log scales between the peek stress intensity factor and the crack depth, Figure 17 shows the crack growth up to the critical depth. The critical depth would be 13.6 mm for extreme loads. This result is somewhat sensitive: if toughness were 1483 MPa$\sqrt{\text{mm}}$, failure would be expected after a depth of 4.5 mm; the same would occur if the load were 91 kNm. This torque, however, is unable to produce enough yielding for the bending failure of an unimpaired tooth. Starting from a 4.5 mm crack in the lower flank, the critical depth would be reached in about 2 years.

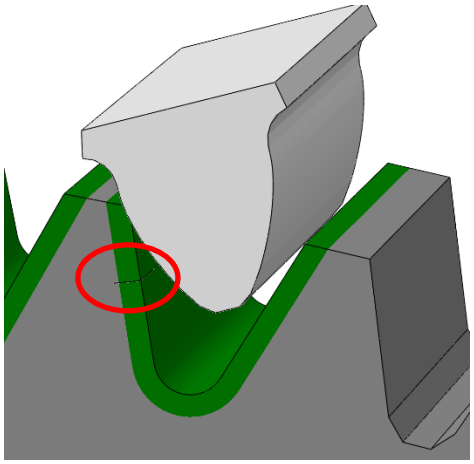

Figure 15. Crack defined in XFEM.

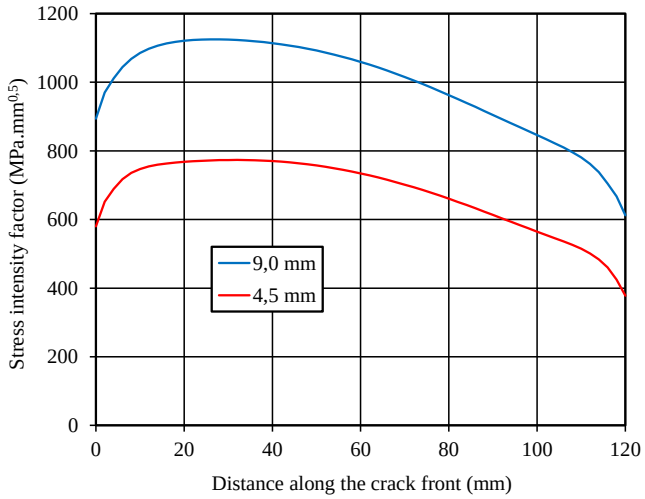

Figure 16. Stress intensity factor along the crack front for fatigue loads.

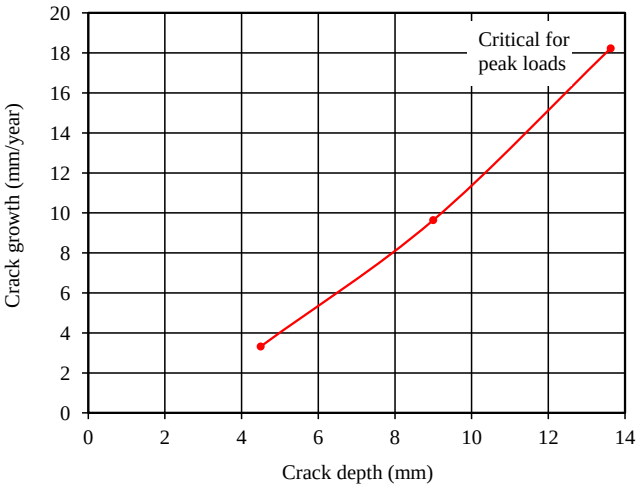

Figure 17. Crack growth.

4. Conclusions

Several problems involving cracking phenomena have been studied using Abaqus and fe-safe. As a result of the work conducted, several conclusions can be offered:

- In relation with the problems experienced by the alurings, the analyses have allowed establishing the causes of the cracks and predicting their occurrence.
- In relation with cracking of the gear rim, it has been seen that cracks are possible near the top land of the tooth, but are not catastrophic. Cracks in the lower face or flank are more dangerous, as they may lead to low-cycle failure.

5. References

1. British Steel, "Determination of fracture toughness from Charpy impact energy: procedure and validation", 1998.

2. Carbide Depot, "Hardness conversion chart". 2017.

3. Göncz, P., Potočnik, R. y Glodež, S., "Fatigue Behaviour of 42CrMo4 Steel under Contact Loading", Procedia Engineering 2, pp. 1991-1999, 2010.

4. Ship Structure Committee, "Fracture Mechanics characterization of Aluminum alloys for marine structural applications", Report no. SSC-448, 2007.

5. SIMULIA, "Abaqus Analysis User's Guide", version 2016, 2016a.

6. SIMULIA, "fe-safe User's Guide", version 2016, 2016b.

7. SIMULIA, "Abaqus/CAE User's Guide", version 2016, 2016c.

8. Taylor, D., "Analysis of fatigue failures in components using the theory of critical distances", Engineering Failure Analysis, Vol. 12, pp. 906-914, 2005.